

The influence of patient size on dose conversion coefficients: a hybrid phantom study for adult cardiac catheterization

This article has been downloaded from IOPscience. Please scroll down to see the full text article.

2009 Phys. Med. Biol. 54 3613

(<http://iopscience.iop.org/0031-9155/54/12/001>)

View [the table of contents for this issue](#), or go to the [journal homepage](#) for more

Download details:

IP Address: 38.107.179.210

The article was downloaded on 16/02/2012 at 02:48

Please note that [terms and conditions apply](#).

The influence of patient size on dose conversion coefficients: a hybrid phantom study for adult cardiac catheterization

Perry Johnson¹, Choonsik Lee¹, Kevin Johnson², Daniel Siragusa³
and Wesley E Bolch^{4,5}

¹ Department of Nuclear and Radiological Engineering, University of Florida, Gainesville, FL 32611, USA

² Department of Radiology, University of Florida, Jacksonville, FL 32209, USA

³ Department of Radiology, Division of Vascular Interventional Radiology, University of Florida, Jacksonville, FL 32209, USA

⁴ Departments of Nuclear and Radiological and Biomedical Engineering, University of Florida, Gainesville, FL 32611, USA

E-mail: wbolch@ufl.edu

Received 31 January 2009, in final form 10 April 2009

Published 21 May 2009

Online at stacks.iop.org/PMB/54/3613

Abstract

In this study, the influence of patient size on organ and effective dose conversion coefficients (DCCs) was investigated for a representative interventional fluoroscopic procedure—cardiac catheterization. The study was performed using hybrid phantoms representing an underweight, average and overweight American adult male. Reference body sizes were determined using the NHANES III database and parameterized based on standing height and total body mass. Organ and effective dose conversion coefficients were calculated for anterior–posterior, posterior–anterior, left anterior oblique and right anterior oblique projections using the Monte Carlo code MCNPX 2.5.0 with the metric dose area product being used as the normalization factor. Results show body size to have a clear influence on DCCs which increased noticeably when body size decreased. It was also shown that if patient size is neglected when choosing a DCC, the organ and effective dose will be underestimated to an underweight patient and will be overestimated to an overweight patient, with errors as large as 113% for certain projections. Results were further compared with those published for a KTMAN-2 Korean patient-specific tomographic phantom. The published DCCs aligned best with the hybrid phantom which most closely matched in overall body size. These results highlighted the need for and the advantages of phantom-patient matching, and it is recommended that hybrid phantoms be used to create a more diverse

⁵ Address for correspondence: Advanced Laboratory for Radiation Dosimetry Studies (ALRADS), Department of Nuclear and Radiological Engineering, University of Florida, Gainesville, FL 32611-8300, USA.

library of patient-dependent anthropomorphic phantoms for medical dose reconstruction.

1. Introduction

Dose conversion coefficients (DCCs) are a widely accepted means for estimating internal organ dose in patients undergoing interventional fluoroscopic procedures. These coefficients, generally determined through Monte Carlo radiation transport simulation, relate the organ absorbed dose for frequently encountered patient/irradiation geometries to a clinically measurable indicator quantity such as dose area product (DAP), entrance air kerma (EAK) or entrance skin dose (ESD). As such, they may be used by healthcare professionals to help manage patient risk. As with any simulation-based quantity, certain assumptions must be made to match the characteristics of a real imaging examination. Examples include the approximation of dynamic imaging sequences by a series of static fields, the use of computer algorithms to estimate the incident x-ray spectrum and the neglect of patient respiratory or cardiac motion. While these assumptions are often justified, the primary assumption inherent to all DCCs is that an *individual* patient can be accurately represented by a computational phantom. The validity of this argument is strongly dependent on phantom type and whether patient-phantom matching is included during phantom selection.

Currently, two types of computational phantoms have been employed for the calculation of DCCs: (1) stylized anatomic models based on geometric descriptions of organ boundaries and outer body contours and (2) tomographic anatomic models based on segmented imaging data of live or cadaveric subjects. Multiple studies have been performed using the former type with the two most significant studies being those published by the US Food and Drug Administration (Stern *et al* 1995) and the British National Radiological Protection Board (Hart *et al* 1994). Dose conversion coefficients based on tomographic models represent a more recent development with extensive publications appearing in the literature within only the last few years (Bozkurt and Bor 2007, Lee *et al* 2006a, Park *et al* 2008, Schlattl *et al* 2007). While each phantom type represents a different approach to patient dosimetry, they share a common disadvantage for the creation of DCCs in that anthropometric variability is difficult to describe. Stylized models offer the ability to modify posture and adjust body morphometry but the resulting phantoms lack anatomical specificity and anthropometric detail. Conversely, tomographic phantoms provide a high fidelity representation of patient anatomy including a genuine outer body contour but are difficult to scale non-uniformly. As such, a limited number of attempts have been made to quantify the sensitivity of DCCs to changes in patient morphometry.

Veit and Zankl (1992, 1993) published two studies in the early 1990s investigating variations in organ dose in pediatric radiology due to changes in patient size. In these studies, the voxel models BABY and CHILD (Veit *et al* 1989) were used to estimate organ dose for a number of anterior–posterior (AP) projections. While these studies were able to show a correlation between organ dose and patient diameter, phantom modification was limited to uniform scaling of the voxel size in different dimensions.

In a more recent study, Tung *et al* (2008) allowed variations in phantom subcutaneous fat thickness through application of various phantom-patient matching techniques based on standard anthropometric parameters. In this work, investigators used semi-empirical formulae based on depth–dose distributions within a computational model of the 35-slice

Alderson-Rando physical phantom (Servomaa *et al* 1989). Patient diameter was altered depending on the mean weight of individuals in the general population that have the same height as that of the patient in question. If patient weight was less than the mean, the phantom contour and organs were scaled uniformly inward in 2D. If patient weight was larger than the mean, subcutaneous fat was added to the outside layer of the virtual patient. The method of simulating underweight and overweight patients was based on statistical studies of human anatomy and represents a shift from pure isometric scaling of a reference phantom. With organ doses calculated for a variety of different patient sizes, selected organ doses were plotted versus body mass index (BMI). A general trend of decreasing organ dose with increasing BMI was shown for a given ESD. Since BMI is roughly proportional to trunk thickness, it was noted that BMI may be used to estimate a size-dependent organ and effective dose.

The results of the Tung *et al* study highlighted many areas where current DCCs may be improved. While voxel phantoms can and have been used to make some of these improvements, they are still limited by a relatively rigid anatomical structure. Research at the *Advanced Laboratory for Radiation Dosimetry Studies* (ALRADS) at the University of Florida has focused on the development of a new type of computational phantom that offers specific advantages for these applications. Hybrid phantoms, first introduced by Lee *et al* (2007), utilize non-uniform rational B-spline (NURBS) surface modeling to describe organ/tissue boundaries. This type of modeling relies on the manipulation of surface control points and thus allows for preservation of anatomical realism while at the same time achieving a level of anthropometric remodeling not previously available in either stylized or tomographic phantoms.

In the present study, the ability of NURBS modeling to create diverse anthropomorphic phantoms is demonstrated through the construction of three phantoms representing an underweight, average and overweight American adult male. These phantoms are then used to investigate the dependence of DCCs on patient size for a representative interventional fluoroscopy procedure—cardiac catheterization. The DCC study by Park *et al* (2008) was used as a template for this work with calculated results compared to those previously published for the individual-specific KTMAN-2 Korean voxel phantom (Lee *et al* 2006b).

2. Materials and methods

2.1. Computational phantoms

The UF hybrid adult male phantom (UFHADM) was used as the base phantom for this study (Lee *et al* 2008). The UFHADM was created based on CT imaging data (330 CT images at 3 mm slice thickness and 512×512 matrix size) taken from a 36 year Korean male cadaver. Due to the fact that the CT data did not include the extremities, images of the arms and legs were collected from high-resolution CT scans (820 slices at 1 mm for the arms and 1099 slices at 1 mm for the legs) of an 18 year male cadaver. Each image was subsequently segmented and imported to the NURBS modeling software RhinocerosTM (McNeel North American, Seattle, WA). NURBS surfaces were used to describe the majority of the phantom including the outer body contour and the boundaries of most internal organs. A limited number of structures, including the skeleton, brain and extrathoracic airways, were difficult to model as NURBS surfaces and were left in their native polygon mesh format. Once the initial modeling was completed, the organ sizes were adjusted to match the reference masses given in ICRP Publication 89 (ICRP 2002). The outer body contour was also modified to

Table 1. Anthropometric parameterization of an underweight, average and overweight American adult male based on the NHANES III database.

Phantom	Standing height (cm)	Total body mass (cm)	Sitting height (cm)	Circumferences (cm)			
				Arm	Thigh	Waist	Buttocks
UFHADM ₅₀₋₁₀	173.2 (50%)	64.1 (10%)	90.2	28.9	46.0	82.0	90.3
UFHADM ₅₀₋₅₀		78.4 (50%)	90.2	32.2	50.5	95.6	98.0
UFHADM ₅₀₋₉₀		97.3 (90%)	90.2	36.3	55.4	112.4	107.6
KTMAN-2	172	68	–	–	–	–	–

match ICRP 89 reference parameters including standing height (176 cm) and total body mass (73 kg).

The ICRP-compliant UFHADM phantom represents the starting point for further anthropometric modeling. In order to create a set of hybrid phantoms specific to a U.S. population, the UFHADM was customized based on the anthropometric data found within the NHANES III database compiled by the U.S. Center for Health Statistics⁶. It includes roughly 30 000 individuals of ages ranging from 2 months to 90 years and lists a variety of primary anthropometric parameters including standing height, sitting height and total body mass, as well as secondary parameters such as waist, buttocks, arm and thigh circumference. From this database, approximately 7000 adult male patients were selected. A histogram was created from their standing height distribution, and a Gaussian fit was used to determine 173.2 cm as the 50th percentile standing height. A further cut to the data was made leaving 820 male adults with a standing height of 173.2 ± 1 cm. In order to parameterize the terms underweight, average and overweight, a histogram was generated from the total body mass distribution of the remaining patients, and a Gaussian fit used to determine 10th (64.1 kg), 50th (78.4 kg) and 90th (97.3 kg) weight percentiles at 50th percentile standing height. Secondary anthropometric parameters for each phantom were selected based upon the average individual having a total body mass within 0.5 kg of each reference value. A list of the anthropometric data for this set of U.S.-based hybrid phantoms is listed in table 1. The acronyms UFHADM₅₀₋₁₀, UFAHDM₅₀₋₅₀ and UFHADM₅₀₋₉₀ are used to indicate the underweight, average and overweight phantoms, respectively, where the first subscripted number denotes the height percentile and the latter denotes the weight percentile within that height subset.

The construction of each phantom followed a procedure developed to maintain both efficiency of method and anatomical realism. To begin, the trunk height of the ICRP 89 compliant UFHADM phantom was uniformly scaled in 3D to match the average sitting height (90.2 cm) of all patients selected at the targeted standing height (173.2 cm). The basis for using trunk height as a first scaling parameter was previously presented in Whalen *et al* (2008) where it was found to be a useful predictor of internal organ volume, at least in pediatric subjects. With the trunk height set, the leg length was next adjusted to achieve the targeted standing height. The next step in phantom modification was to match the secondary parameters listed in table 1. For the average and overweight phantoms, this was achieved by simply altering the control points of the outer body contour, simulating a change in subcutaneous fat thickness and its body distribution. For the underweight phantom, the targeted waist circumference was found to be smaller than allowed by the existing skeletal model. In this case, the anatomical information indicated that further scaling of the torso was necessary. A process similar to that

⁶ <http://www.cdc.gov/nchs/nhanes.htm>.

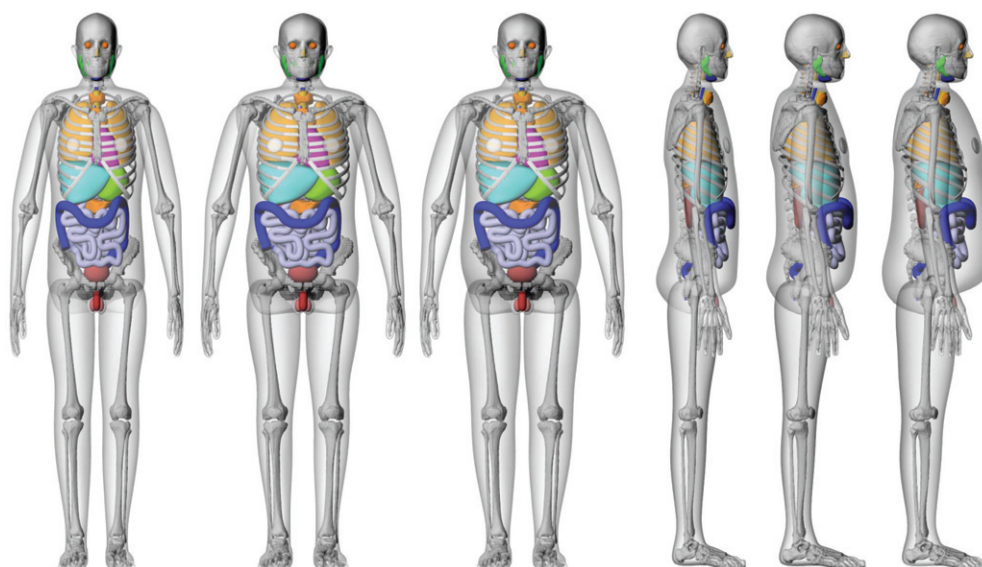


Figure 1. Presentation of the underweight, average and overweight American male adult as defined by the NHANES III database.

(This figure is in colour only in the electronic version)

employed by Tung *et al* (2008) was thus used where the torso was scaled slightly inward in 2D. Secondary parameters were then matched by fine-tuning control points of the outer body contour.

The final step of phantom construction was to match the reference 10th, 50th and 90th weight percentiles. This process was performed simultaneously with phantom voxelization using an in-house MATLAB™ code. One unique aspect of hybrid phantoms is that they can be voxelized at any desired resolution. For this work, a resolution of $2 \times 2 \times 2 \text{ mm}^3$ was chosen based on an approximate skin thickness represented by the phantom's outer voxel layer. Once each phantom was voxelized, total body mass was calculated using the voxelized organ volumes and their corresponding reference densities in ICRU Report 46 (ICRU 1992). Any mass difference was accounted for by adjusting control points in the outer body contour of the pre-voxelized phantom to increase or decrease residual soft tissue. Control points were altered in areas not constrained by secondary parameters, e.g. upper torso, lower legs and arms. After each hybrid-NURBS phantom was finalized, voxelization was again performed, and a MCNPX lattice structure created using another in-house MATLAB™ code. Figure 1 shows the final versions of the UFHADM₅₀₋₁₀, UFHADM₅₀₋₅₀ and UFHADM₅₀₋₉₀.

The anthropometrically modified hybrid phantoms represent what may be considered a new class of *patient-dependent* phantoms, the theory being that patients will eventually be matched to members of a broad phantom library based on external anthropometric measurements. Patient-dependent phantoms increase patient specificity while maintaining generality to represent a diverse population. This balance is lacking in both stylized and tomographic reference phantoms which are too generic to represent any single patient, and in individual-specific voxel phantoms which may present a body habitus too divergent from the patient for which the dose estimate is sought.

2.2. Exam parameters

To make consistent comparisons with the DCCs derived from KTMAN-2, the examination simulated by Park *et al* (2008) was replicated. This examination included combinations of four beam projections and three beam spectra. The four beam projections were divided into two sets: AP/posterior–anterior (PA) and left anterior oblique (LAO)/right anterior oblique (RAO). The nomenclature for oblique angles is defined by the location of the detector; accordingly, the source term for a left anterior oblique is actually located patient-right/posterior. Both oblique projections were oriented at a 45° angle between the coronal and sagittal planes. The center of mass of the heart was used as the isocenter for all projections, and the source-to-isocenter distance was fixed at 59.8 cm. For the AP/PA set, the field size at isocenter was set at 12 × 12 cm². For the LAO/RAO set, the field size at isocenter was set at 14 × 14 cm². To make these field sizes, an adjustable lead collimator was positioned 10 cm from the source term. Both the phantom and collimator were located within an air-filled medium. In order to remain consistent with the comparison study, a patient table was not simulated.

The SPEC 78 spectrum generator (Cranley *et al* 1997) was used to characterize the diagnostic beam. For each x-ray spectrum, tungsten was used as the target material, aluminum was used for total filtration and the anode angle was set at 12°. The three spectra differed in their combination of peak tube voltage and filtration thickness. The first spectrum was calculated using a peak tube voltage of 60 kVp and 3.5 mm Al, the second at 90 kVp and 4 mm Al, and the third using 120 kVp and 4.3 mm Al. These spectra were originally presented in Stern *et al* (1995) as representative spectra for cardiac catheterization.

2.3. Monte Carlo simulation and dose standardization

Photon transport was performed using the general-purpose Monte Carlo code MCNPX 2.5.0 (Pelowitz 2005). The F6 kerma tally (MeV g⁻¹) was used to approximate energy deposition in 24 organ volumes covering a majority of the organs of interest as defined in ICRP Publication 103 (ICRP 2007). This tally provides an estimation of kerma which was used as an analogue for absorbed dose in this study. For red bone marrow (RBM) and bone surface (BS) dose, the F4 fluence tally (particles cm⁻²) was used along with an updated version of the recently published fluence-to-dose response functions (DRFs) by Eckerman *et al* (2008). The new DRFs represent an improvement over their 1985 counterparts (Eckerman 1985) as they are based upon bone-dependent micro-CT imaging data and associated electron absorbed fraction data. To estimate the absorbed dose to RBM, the average fluence for each bone site was tabulated and multiplied by the corresponding DRF. Individual bone doses were then multiplied by the fraction of total RBM found locally in each skeletal site. The dose to RBM was calculated by summing the weighted doses. This procedure was repeated for the bone surface dose.

Simulations were performed on the ALRADS cluster comprised of 9 AMD Dual Opteron 2216 processors with 4 GB of RAM and 4 AMD Quad Opteron 2350 processors with 8 GB of RAM. All runs (combinations of x-ray spectrum, phantom weight percentile and projection angle) were made using 10⁸ photon histories with each taking between 350 and 600 min for completion depending on cluster usage. The number of histories was chosen to reduce statistical errors below 1%. This was achieved for all in-field and near-field organs, with only some of the smaller and out-of-field organs (i.e., gonads, bladder wall and prostate) displaying large errors.

Organ dose conversion coefficients were calculated using the metric dose–area product. The DAP is widely used for this purpose because it can be conveniently measured in the clinic and provides an estimate of beam intensity. The DAP was measured both 15 cm from the

source on the tube side and 8 cm from the patient's skin on the detector side. The DAP meter was modeled as a 1 cm thick rectangular volume with an area equivalent to the respective beam area at each location. To ensure that tabulated organ dose conversion coefficients are clinically relevant, they are typically reported as organ dose normalized by a tube-side DAP reading. Due to the fact that beam intensity must be either increased or decreased for larger or smaller patients to achieve the same image quality, it is more intuitive, however, to normalize organ dose by a detector-side DAP reading. Both methods were employed in this study, while the DCCs normalized by the detector-side DAP were used to help draw conclusions regarding the influence of patient size on organ absorbed dose.

Organ dose conversion coefficients are often standardized using the concept of effective dose. The ICRP defines effective dose as the sum of the tissue-weighted equivalent doses over all organs. As tissue weighting factors are given by the ICRP independent of age and gender, it is emphasized that effective dose should not be used to assign risk to specific patients. More important is the actual dose to each organ which can be used to assess the probability of cancer induction when paired with the appropriate carcinogenic models. Also due to the fact that the tissue weighting factors are given independent of gender, effective dose is designated only for the reference person. This requires an averaging of dose from both a male and female phantom with specific sex organs for each. This type of averaging was not included in this study because the UFHADM-based patient-dependent phantoms are not reference and thus have no reference female counterpart.

With this in mind, male-only effective doses were calculated in this study only to provide a standard for comparison between the different Monte Carlo runs and literature values. Organ doses were multiplied by their respective tissue weighting factors as listed in ICRP Publication 103. All organs of interest were included with the exception of muscle and lymph nodes which were as yet defined in the original hybrid phantom. The dose to the phantom's *residual soft tissue* was used as a surrogate for both tissues. This method was based on the assumption that both muscle and lymph nodes are widely distributed and could be represented with an equally distributed tissue surrogate. The resulting effective dose estimates were divided by the tube-side DAP reading and reported as effective dose conversion coefficients.

3. Results

Organ and effective dose conversion coefficients for 36 distinct Monte Carlo runs are listed in tables 2–5. As anticipated, in-field and near-field organs including the heart, lungs, stomach, liver, esophagus, spleen, thymus and breasts received the highest absorbed doses, while out-of-field organs such as the brain, bladder, prostate and gonads received substantially lower doses. Patient/tube geometry played an important role in dictating the distribution of organ dose as organs located closer to the entrance surface received higher doses. This can be seen in that organs located patient-left such as the heart, stomach and spleen received higher doses during RAO projections, while organs located patient-right such as the liver received higher doses during LAO projections. Another tissue showing a strong dependence on tube angle was breast tissue which received considerably higher doses during AP projections as it was located near the source and directly in the field of view. For these runs, the contribution from breast dose accounted for roughly half the effective dose.

Several general trends were observed when patient size was modified and tube potential altered. First, organ and effective dose conversion coefficients increased noticeably when total body mass decreased. This was due to a reduction in soft tissue organ shielding. The

Table 2. Organ dose conversion coefficients (mGy per Gy cm²) and effective dose conversion coefficient (mSv per Gy cm²) for AP projections.

AP projection	60 kVp 3.5 mm Al UFHADM weight percentile			90 kVp 4.0 mm Al UFHADM weight percentile			120 kVp 4.3 mm Al UFHADM weight percentile		
	10%	50%	90%	10%	50%	90%	10%	50%	90%
Organs									
Colon	6.04E-03 (0.67%)	5.51E-03 (0.63%)	5.61E-03 (0.63%)	1.91E-02 (0.41%)	1.77E-02 (0.38%)	1.96E-02 (0.37%)	3.02E-02 (0.34%)	2.86E-02 (0.31%)	3.21E-02 (0.30%)
Lung	4.70E-01 (0.05%)	2.83E-01 (0.06%)	1.45E-01 (0.08%)	8.07E-01 (0.04%)	5.23E-01 (0.05%)	3.16E-01 (0.06%)	1.02E+00 (0.04%)	6.81E-01 (0.04%)	4.38E-01 (0.05%)
Stomach	2.33E-01 (0.15%)	1.85E-01 (0.15%)	1.10E-01 (0.19%)	4.71E-01 (0.11%)	3.94E-01 (0.11%)	2.68E-01 (0.13%)	6.30E-01 (0.10%)	5.38E-01 (0.10%)	3.85E-01 (0.11%)
Bladder	8.88E-05 (10.14%)	7.53E-05 (9.21%)	6.52E-05 (10.62%)	4.92E-04 (4.65%)	4.52E-04 (4.37%)	4.53E-04 (4.48%)	1.09E-03 (3.34%)	1.08E-03 (2.93%)	9.94E-04 (3.08%)
Liver	1.74E-01 (0.10%)	1.32E-01 (0.10%)	8.28E-02 (0.13%)	3.56E-01 (0.08%)	2.82E-01 (0.08%)	2.02E-01 (0.09%)	4.78E-01 (0.07%)	3.85E-01 (0.07%)	2.90E-01 (0.08%)
Esophagus	2.56E-01 (0.21%)	1.77E-01 (0.23%)	8.71E-02 (0.32%)	5.84E-01 (0.15%)	4.37E-01 (0.16%)	2.47E-01 (0.21%)	8.20E-01 (0.13%)	6.31E-01 (0.13%)	3.78E-01 (0.17%)
Thyroid	2.34E-02 (1.26%)	2.04E-02 (1.19%)	1.81E-02 (1.25%)	6.86E-02 (0.79%)	6.31E-02 (0.73%)	5.96E-02 (0.75%)	1.03E-01 (0.66%)	9.74E-02 (0.61%)	9.45E-02 (0.62%)
Gonads	4.71E-05 (20.47%)	7.74E-05 (18.29%)	3.31E-05 (24.10%)	1.62E-04 (14.03%)	1.85E-04 (11.94%)	7.79E-05 (17.06%)	2.88E-04 (10.19%)	2.95E-04 (9.44%)	1.56E-04 (12.40%)
Skin	8.07E-02 (0.03%)	7.26E-02 (0.03%)	6.56E-02 (0.03%)	9.73E-02 (0.03%)	8.67E-02 (0.03%)	7.77E-02 (0.03%)	1.08E-01 (0.03%)	9.59E-02 (0.03%)	8.56E-02 (0.03%)
Brain	2.68E-04 (2.77%)	2.64E-04 (2.40%)	2.22E-04 (2.65%)	1.08E-03 (1.54%)	1.18E-03 (1.29%)	1.04E-03 (1.39%)	2.04E-03 (1.16%)	2.27E-03 (0.98%)	2.00E-03 (1.05%)
Kidneys	1.27E-02 (0.62%)	1.00E-02 (0.63%)	6.58E-03 (0.77%)	4.22E-02 (0.38%)	3.54E-02 (0.37%)	2.63E-02 (0.43%)	6.70E-02 (0.31%)	5.85E-02 (0.30%)	4.48E-02 (0.34%)
Salivary glands	2.55E-03 (1.94%)	3.45E-03 (1.46%)	2.40E-03 (1.81%)	7.59E-03 (1.21%)	9.65E-03 (0.95%)	7.67E-03 (1.08%)	1.22E-02 (0.98%)	1.48E-02 (0.79%)	1.27E-02 (0.86%)
Adrenals	4.52E-02 (0.93%)	3.31E-02 (0.96%)	1.95E-02 (1.24%)	1.29E-01 (0.58%)	9.96E-02 (0.59%)	6.67E-02 (0.73%)	1.94E-01 (0.49%)	1.57E-01 (0.49%)	1.09E-01 (0.59%)
Gall bladder	2.90E-02 (0.83%)	2.46E-02 (0.80%)	1.88E-02 (0.91%)	8.47E-02 (0.52%)	7.63E-02 (0.49%)	6.24E-02 (0.54%)	1.29E-01 (0.44%)	1.18E-01 (0.41%)	9.97E-02 (0.44%)
Heart wall	1.84E+00 (0.04%)	1.56E+00 (0.04%)	7.35E-01 (0.06%)	2.99E+00 (0.04%)	2.60E+00 (0.04%)	1.43E+00 (0.05%)	3.69E+00 (0.04%)	3.24E+00 (0.04%)	1.91E+00 (0.04%)
Prostate	1.84E-05 (57.11%)	2.19E-05 (36.37%)	7.42E-06 (46.71%)	1.72E-04 (17.27%)	1.32E-04 (16.98%)	1.17E-04 (18.88%)	4.24E-04 (12.86%)	3.35E-04 (10.94%)	3.02E-04 (12.61%)
SI wall	2.86E-03 (0.64%)	2.63E-03 (0.59%)	2.33E-03 (0.64%)	1.05E-02 (0.38%)	1.02E-02 (0.35%)	9.72E-03 (0.36%)	1.76E-02 (0.31%)	1.74E-02 (0.28%)	1.70E-02 (0.28%)
Spleen	1.47E-01 (0.26%)	1.02E-01 (0.28%)	5.48E-02 (0.38%)	3.45E-01 (0.19%)	2.56E-01 (0.19%)	1.57E-01 (0.25%)	4.84E-01 (0.16%)	3.72E-01 (0.17%)	2.38E-01 (0.21%)
Thymus	1.65E-01 (0.42%)	1.51E-01 (0.39%)	9.28E-02 (0.49%)	3.55E-01 (0.30%)	3.37E-01 (0.28%)	2.38E-01 (0.33%)	4.82E-01 (0.26%)	4.63E-01 (0.24%)	3.47E-01 (0.28%)
Breasts	1.92E+00 (0.08%)	9.27E-01 (0.11%)	7.76E-01 (0.12%)	2.40E+00 (0.08%)	1.21E+00 (0.10%)	1.05E+00 (0.11%)	2.71E+00 (0.07%)	1.40E+00 (0.09%)	1.22E+00 (0.10%)
ET region	1.75E-02 (1.24%)	1.54E-02 (1.16%)	1.29E-02 (1.25%)	4.96E-02 (0.78%)	4.66E-02 (0.71%)	4.18E-02 (0.75%)	7.43E-02 (0.65%)	7.16E-02 (0.59%)	6.64E-02 (0.61%)
Oral mucosa	2.01E-03 (5.26%)	3.37E-03 (3.97%)	1.94E-03 (4.88%)	6.49E-03 (3.37%)	9.50E-03 (2.46%)	6.56E-03 (2.92%)	1.06E-02 (2.64%)	1.45E-02 (2.03%)	1.13E-02 (2.33%)
Pancreas	1.38E-02 (0.86%)	1.32E-02 (0.78%)	1.10E-02 (0.86%)	4.59E-02 (0.52%)	4.52E-02 (0.47%)	4.00E-02 (0.50%)	7.25E-02 (0.43%)	7.26E-02 (0.38%)	6.60E-02 (0.40%)
Bone marrow	6.68E-02 (1.08%)	5.24E-02 (1.09%)	2.66E-02 (1.25%)	1.44E-01 (0.51%)	1.14E-01 (0.49%)	6.83E-02 (0.54%)	2.08E-01 (0.37%)	1.66E-01 (0.35%)	1.06E-01 (0.36%)
Bone surfaces	4.21E-02 (2.15%)	3.25E-02 (2.06%)	1.67E-02 (2.68%)	9.27E-02 (1.43%)	7.23E-02 (1.34%)	4.38E-02 (1.56%)	1.31E-01 (1.09%)	1.03E-01 (0.99%)	6.63E-02 (1.10%)
Effective dose	3.68E-01 (1.81%)	2.10E-01 (1.57%)	1.46E-01 (2.05%)	5.47E-01 (1.16%)	3.43E-01 (0.99%)	2.51E-01 (1.40%)	6.68E-01 (0.84%)	4.34E-01 (0.78%)	3.26E-01 (1.01%)

Table 3. Organ dose conversion coefficients (mGy per Gy cm²) and effective dose conversion coefficient (mSv per Gy cm²) for PA projections.

AP projection	60 kVp 3.5 mm Al UFHADM weight percentile			90 kVp 4.0 mm Al UFHADM weight percentile			120 kVp 4.3 mm Al UFHADM weight percentile		
	10%	50%	90%	10%	50%	90%	10%	50%	90%
Organs									
Colon	2.46E-03 (1.04%)	1.72E-03 (1.11%)	1.81E-03 (1.08%)	1.03E-02 (0.55%)	7.68E-03 (0.57%)	8.46E-03 (0.55%)	1.80E-02 (0.43%)	1.41E-02 (0.44%)	1.56E-02 (0.42%)
Lung	5.69E-01 (0.04%)	3.75E-01 (0.05%)	3.63E-01 (0.05%)	9.55E-01 (0.04%)	6.55E-01 (0.04%)	6.44E-01 (0.04%)	1.20E+00 (0.04%)	8.38E-01 (0.04%)	8.28E-01 (0.04%)
Stomach	1.27E-01 (0.20%)	8.70E-02 (0.22%)	8.22E-02 (0.23%)	2.89E-01 (0.15%)	2.13E-01 (0.15%)	2.07E-01 (0.16%)	4.07E-01 (0.13%)	3.10E-01 (0.13%)	3.03E-01 (0.13%)
Bladder	5.31E-05 (12.27%)	4.49E-05 (12.44%)	3.61E-05 (13.66%)	3.83E-04 (5.31%)	3.46E-04 (4.95%)	3.06E-04 (5.16%)	9.01E-04 (3.60%)	7.95E-04 (3.44%)	8.30E-04 (3.40%)
Liver	6.28E-02 (0.17%)	3.26E-02 (0.20%)	3.17E-02 (0.20%)	1.70E-01 (0.11%)	1.03E-01 (0.13%)	1.02E-01 (0.13%)	2.53E-01 (0.10%)	1.62E-01 (0.11%)	1.62E-01 (0.11%)
Esophagus	2.99E-01 (0.19%)	1.99E-01 (0.22%)	1.92E-01 (0.22%)	7.30E-01 (0.13%)	5.42E-01 (0.14%)	5.26E-01 (0.14%)	1.05E+00 (0.11%)	8.14E-01 (0.12%)	7.93E-01 (0.12%)
Thyroid	1.54E-02 (1.56%)	1.07E-02 (1.66%)	1.16E-02 (1.58%)	5.16E-02 (0.91%)	3.98E-02 (0.93%)	4.34E-02 (0.89%)	8.15E-02 (0.74%)	6.47E-02 (0.74%)	7.11E-02 (0.71%)
Gonads	8.54E-06 (46.73%)	1.68E-05 (46.70%)	9.28E-06 (46.11%)	8.53E-05 (22.91%)	6.97E-05 (17.65%)	3.94E-05 (21.60%)	1.48E-04 (14.18%)	1.36E-04 (14.16%)	1.19E-04 (14.42%)
Skin	7.43E-02 (0.03%)	6.63E-02 (0.03%)	5.92E-02 (0.03%)	9.00E-02 (0.03%)	7.93E-02 (0.03%)	7.03E-02 (0.03%)	1.01E-01 (0.03%)	8.81E-02 (0.03%)	7.78E-02 (0.03%)
Brain	3.15E-04 (2.59%)	2.85E-04 (2.44%)	2.82E-04 (2.40%)	1.20E-03 (1.47%)	1.16E-03 (1.32%)	1.20E-03 (1.31%)	2.14E-03 (1.15%)	2.22E-03 (1.00%)	2.23E-03 (1.01%)
Kidneys	1.43E-02 (0.60%)	1.21E-02 (0.58%)	1.20E-02 (0.58%)	4.59E-02 (0.36%)	4.05E-02 (0.35%)	4.14E-02 (0.35%)	7.21E-02 (0.30%)	6.54E-02 (0.28%)	6.76E-02 (0.28%)
Salivary glands	1.53E-03 (2.47%)	1.26E-03 (2.41%)	1.37E-03 (2.36%)	5.56E-03 (1.40%)	5.31E-03 (1.27%)	5.56E-03 (1.25%)	9.43E-03 (1.10%)	9.12E-03 (1.00%)	9.77E-03 (0.97%)
Adrenals	6.82E-02 (0.73%)	5.65E-02 (0.71%)	5.66E-02 (0.71%)	1.79E-01 (0.48%)	1.54E-01 (0.46%)	1.54E-01 (0.46%)	2.60E-01 (0.41%)	2.31E-01 (0.39%)	2.32E-01 (0.39%)
Gall bladder	1.31E-02 (1.22%)	8.32E-03 (1.36%)	8.10E-03 (1.33%)	4.87E-02 (0.69%)	3.60E-02 (0.71%)	3.57E-02 (0.71%)	8.07E-02 (0.55%)	6.22E-02 (0.56%)	6.33E-02 (0.56%)
Heart wall	5.87E-01 (0.07%)	3.87E-01 (0.08%)	3.69E-01 (0.08%)	1.18E+00 (0.06%)	8.36E-01 (0.06%)	8.08E-01 (0.06%)	1.60E+00 (0.05%)	1.17E+00 (0.05%)	1.13E+00 (0.05%)
Prostate	2.58E-05 (44.78%)	2.64E-05 (37.69%)	1.86E-05 (54.46%)	2.14E-04 (15.53%)	1.45E-04 (14.13%)	1.30E-04 (19.35%)	4.64E-04 (11.40%)	3.68E-04 (10.72%)	3.02E-04 (11.55%)
SI wall	1.44E-03 (0.89%)	1.07E-03 (0.92%)	1.07E-03 (0.92%)	6.53E-03 (0.48%)	5.32E-03 (0.47%)	5.53E-03 (0.47%)	1.18E-02 (0.38%)	1.01E-02 (0.36%)	1.06E-02 (0.36%)
Spleen	3.03E-01 (0.19%)	2.31E-01 (0.19%)	2.22E-01 (0.20%)	5.90E-01 (0.15%)	4.74E-01 (0.15%)	4.67E-01 (0.15%)	7.70E-01 (0.13%)	6.33E-01 (0.13%)	6.26E-01 (0.13%)
Thymus	6.72E-02 (0.59%)	4.52E-02 (0.65%)	4.54E-02 (0.65%)	1.82E-01 (0.39%)	1.36E-01 (0.41%)	1.37E-01 (0.40%)	2.71E-01 (0.33%)	2.06E-01 (0.34%)	2.13E-01 (0.33%)
Breasts	1.01E-01 (0.31%)	4.26E-02 (0.44%)	2.03E-02 (0.63%)	2.47E-01 (0.21%)	1.13E-01 (0.29%)	6.27E-02 (0.40%)	3.74E-01 (0.18%)	1.78E-01 (0.25%)	1.04E-01 (0.33%)
ET region	1.11E-02 (1.54%)	7.78E-03 (1.64%)	8.31E-03 (1.59%)	3.70E-02 (0.91%)	2.93E-02 (0.90%)	3.06E-02 (0.89%)	5.88E-02 (0.74%)	4.79E-02 (0.73%)	5.14E-02 (0.70%)
Oral mucosa	7.08E-04 (10.11%)	5.54E-04 (9.51%)	5.75E-04 (9.04%)	3.67E-03 (4.78%)	3.26E-03 (4.22%)	3.42E-03 (4.47%)	6.20E-03 (3.42%)	6.30E-03 (3.05%)	6.34E-03 (3.16%)
Pancreas	6.54E-03 (1.24%)	4.91E-03 (1.27%)	4.86E-03 (1.28%)	2.72E-02 (0.67%)	2.21E-02 (0.66%)	2.26E-02 (0.66%)	4.64E-02 (0.53%)	3.97E-02 (0.52%)	4.04E-02 (0.51%)
Bone marrow	1.20E-01 (0.86%)	9.03E-02 (0.89%)	8.69E-02 (1.09%)	2.49E-01 (0.46%)	1.99E-01 (0.45%)	1.94E-01 (0.50%)	3.53E-01 (0.35%)	2.89E-01 (0.32%)	2.83E-01 (0.34%)
Bone surfaces	7.80E-02 (2.29%)	5.65E-02 (2.14%)	5.45E-02 (2.81%)	1.61E-01 (1.54%)	1.24E-01 (1.39%)	1.22E-01 (1.74%)	2.21E-01 (1.17%)	1.75E-01 (1.07%)	1.72E-01 (1.25%)
Effective dose	1.39E-01 (3.81%)	9.07E-02 (3.80%)	8.50E-02 (3.78%)	2.76E-01 (1.86%)	1.91E-01 (1.44%)	1.81E-01 (1.76%)	3.76E-01 (1.15%)	2.67E-01 (1.15%)	2.54E-01 (1.17%)

Table 4. Organ dose conversion coefficients (mGy per Gy cm²) and effective dose conversion coefficient (mSv per Gy cm²) for LAO projections.

LAO projection	60 kVp 3.5 mm Al UFHADM weight percentile			90 kVp 4.0 mm Al UFHADM weight percentile			120 kVp 1.3 mm Al UFHADM weight percentile		
	10%	50%	90%	10%	50%	90%	10%	50%	90%
Organs									
Colon	2.24E-03 (0.90%)	1.58E-03 (0.96%)	1.62E-03 (0.95%)	9.48E-03 (0.48%)	7.31E-03 (0.49%)	7.93E-03 (0.48%)	1.68E-02 (0.38%)	1.33E-02 (0.38%)	1.48E-02 (0.37%)
Lung	7.01E-01 (0.04%)	5.62E-01 (0.04%)	5.33E-01 (0.04%)	1.17E+00 (0.03%)	9.53E-01 (0.03%)	9.18E-01 (0.03%)	1.46E+00 (0.03%)	1.20E+00 (0.03%)	1.17E+00 (0.03%)
Stomach	4.05E-02 (0.30%)	2.21E-02 (0.36%)	2.12E-02 (0.37%)	1.27E-01 (0.18%)	7.71E-02 (0.21%)	7.56E-02 (0.21%)	2.01E-01 (0.15%)	1.27E-01 (0.17%)	1.26E-01 (0.17%)
Bladder	6.29E-05 (10.33%)	3.74E-05 (11.03%)	3.15E-05 (12.16%)	3.67E-04 (4.56%)	3.59E-04 (4.31%)	3.18E-04 (4.41%)	8.75E-04 (3.05%)	8.78E-04 (2.84%)	8.09E-04 (2.88%)
Liver	2.40E-01 (0.07%)	1.85E-01 (0.07%)	1.71E-01 (0.08%)	4.73E-01 (0.06%)	3.82E-01 (0.06%)	3.62E-01 (0.06%)	6.30E-01 (0.05%)	5.18E-01 (0.05%)	4.97E-01 (0.05%)
Esophagus	3.44E-01 (0.15%)	2.54E-01 (0.17%)	2.43E-01 (0.17%)	7.41E-01 (0.11%)	5.78E-01 (0.12%)	5.58E-01 (0.12%)	1.03E+00 (0.10%)	8.21E-01 (0.10%)	7.97E-01 (0.10%)
Thyroid	2.14E-02 (1.09%)	1.75E-02 (1.07%)	1.83E-02 (1.05%)	6.46E-02 (0.68%)	5.54E-02 (0.65%)	5.96E-02 (0.63%)	9.89E-02 (0.56%)	8.71E-02 (0.54%)	9.47E-02 (0.52%)
Gonads	1.30E-05 (29.07%)	1.86E-05 (30.69%)	9.72E-06 (49.20%)	7.00E-05 (17.68%)	6.78E-05 (15.61%)	4.12E-05 (19.35%)	1.62E-04 (11.24%)	1.37E-04 (11.37%)	1.31E-04 (11.36%)
Skin	9.84E-02 (0.02%)	8.83E-02 (0.02%)	7.94E-02 (0.02%)	1.16E-01 (0.02%)	1.04E-01 (0.02%)	9.29E-02 (0.02%)	1.28E-01 (0.02%)	1.14E-01 (0.02%)	1.02E-01 (0.02%)
Brain	2.97E-04 (2.29%)	2.58E-04 (2.16%)	2.64E-04 (2.11%)	1.22E-03 (1.25%)	1.16E-03 (1.12%)	1.21E-03 (1.11%)	2.26E-03 (0.96%)	2.37E-03 (0.83%)	2.38E-03 (0.83%)
Kidneys	1.35E-02 (0.53%)	1.15E-02 (0.51%)	1.14E-02 (0.51%)	4.42E-02 (0.32%)	3.87E-02 (0.31%)	3.94E-02 (0.30%)	7.06E-02 (0.26%)	6.26E-02 (0.25%)	6.44E-02 (0.25%)
Salivary glands	1.82E-03 (1.95%)	1.76E-03 (1.73%)	1.80E-03 (1.74%)	6.44E-03 (1.11%)	6.67E-03 (0.97%)	6.77E-03 (0.96%)	1.08E-02 (0.88%)	1.13E-02 (0.77%)	1.20E-02 (0.75%)
Adrenals	6.15E-02 (0.65%)	4.89E-02 (0.65%)	4.81E-02 (0.65%)	1.63E-01 (0.43%)	1.35E-01 (0.42%)	1.34E-01 (0.42%)	2.39E-01 (0.36%)	2.01E-01 (0.35%)	2.01E-01 (0.35%)
Gall bladder	2.23E-02 (0.79%)	1.86E-02 (0.77%)	1.79E-02 (0.78%)	7.17E-02 (0.48%)	6.30E-02 (0.45%)	6.20E-02 (0.46%)	1.13E-01 (0.39%)	1.01E-01 (0.37%)	1.00E-01 (0.37%)
Heart wall	3.00E-01 (0.08%)	2.08E-01 (0.09%)	1.98E-01 (0.09%)	6.73E-01 (0.06%)	4.89E-01 (0.06%)	4.74E-01 (0.06%)	9.50E-01 (0.05%)	7.05E-01 (0.06%)	6.89E-01 (0.06%)
Prostate	1.91E-05 (33.42%)	2.26E-05 (34.18%)	1.05E-05 (45.11%)	1.86E-04 (15.85%)	1.50E-04 (14.21%)	8.40E-05 (17.38%)	4.32E-04 (9.94%)	2.98E-04 (9.76%)	3.08E-04 (9.85%)
SI wall	1.77E-03 (0.68%)	1.46E-03 (0.66%)	1.44E-03 (0.67%)	7.41E-03 (0.38%)	6.57E-03 (0.36%)	6.64E-03 (0.36%)	1.31E-02 (0.30%)	1.18E-02 (0.29%)	1.23E-02 (0.28%)
Spleen	7.22E-02 (0.33%)	2.00E-02 (0.55%)	2.05E-02 (0.55%)	1.95E-01 (0.22%)	7.34E-02 (0.32%)	7.45E-02 (0.32%)	2.94E-01 (0.18%)	1.22E-01 (0.26%)	1.24E-01 (0.25%)
Thymus	7.31E-02 (0.49%)	5.42E-02 (0.51%)	5.35E-02 (0.51%)	1.90E-01 (0.32%)	1.51E-01 (0.33%)	1.52E-01 (0.33%)	2.83E-01 (0.27%)	2.28E-01 (0.27%)	2.31E-01 (0.27%)
Breasts	4.40E-02 (0.43%)	2.55E-02 (0.51%)	1.26E-02 (0.72%)	1.18E-01 (0.28%)	7.27E-02 (0.33%)	4.23E-02 (0.43%)	1.82E-01 (0.24%)	1.15E-01 (0.27%)	7.10E-02 (0.35%)
ET region	1.76E-02 (1.05%)	1.51E-02 (1.00%)	1.53E-02 (0.99%)	5.08E-02 (0.66%)	4.43E-02 (0.62%)	4.69E-02 (0.61%)	7.57E-02 (0.55%)	6.85E-02 (0.51%)	7.31E-02 (0.50%)
Oral mucosa	1.11E-03 (6.12%)	9.30E-04 (5.97%)	1.02E-03 (6.13%)	4.16E-03 (3.46%)	4.40E-03 (2.98%)	4.43E-03 (3.07%)	7.90E-03 (2.70%)	8.21E-03 (2.29%)	8.11E-03 (2.36%)
Pancreas	7.07E-03 (1.03%)	5.78E-03 (1.02%)	5.67E-03 (1.04%)	2.82E-02 (0.57%)	2.43E-02 (0.55%)	2.41E-02 (0.55%)	4.81E-02 (0.45%)	4.21E-02 (0.43%)	4.20E-02 (0.43%)
Bone marrow	1.09E-01 (0.72%)	8.31E-02 (0.68%)	8.06E-02 (0.85%)	2.25E-01 (0.39%)	1.73E-01 (0.36%)	1.70E-01 (0.40%)	3.19E-01 (0.28%)	2.48E-01 (0.26%)	2.46E-01 (0.28%)
Bone surfaces	8.38E-02 (1.87%)	6.79E-02 (1.60%)	6.61E-02 (2.11%)	1.67E-01 (1.28%)	1.36E-01 (1.17%)	1.34E-01 (1.45%)	2.26E-01 (0.99%)	1.85E-01 (0.89%)	1.83E-01 (1.05%)
Effective dose	1.40E-01 (2.40%)	1.07E-01 (2.53%)	1.01E-01 (4.00%)	2.67E-01 (1.44%)	2.08E-01 (1.27%)	1.98E-01 (1.57%)	3.58E-01 (0.92%)	2.82E-01 (0.93%)	2.71E-01 (0.93%)

Table 5. Organ dose conversion coefficients (mGy per Gy cm²) and effective dose conversion coefficient (mSv per Gy cm²) for RAO projections.

RAO projection	60 kVp 3.5 mm Al UFHADM weight percentile			90 kVp 4.0 mm Al UFHADM weight percentile			120 kVp 4.3 mm Al JFHADM weight percentile		
	10%	50%	90%	10%	50%	90%	10%	50%	90%
Organs									
Colon	3.77E-03 (0.73%)	3.16E-03 (0.71%)	3.18E-03 (0.71%)	1.36E-02 (0.42%)	1.19E-02 (0.40%)	1.28E-02 (0.39%)	2.27E-02 (0.33%)	2.02E-02 (0.32%)	2.22E-02 (0.31%)
Lung	6.27E-01 (0.03%)	5.19E-01 (0.03%)	4.92E-01 (0.03%)	1.04E+00 (0.03%)	8.72E-01 (0.03%)	8.41E-01 (0.03%)	1.31E+00 (0.03%)	1.10E+00 (0.02%)	1.07E+00 (0.03%)
Stomach	2.37E-01 (0.13%)	1.93E-01 (0.13%)	1.78E-01 (0.13%)	4.77E-01 (0.10%)	4.06E-01 (0.09%)	3.85E-01 (0.10%)	6.39E-01 (0.09%)	5.54E-01 (0.08%)	5.32E-01 (0.09%)
Bladder	6.13E-05 (10.65%)	5.64E-05 (9.80%)	4.32E-05 (10.55%)	4.26E-04 (4.26%)	4.07E-04 (3.90%)	3.54E-04 (4.25%)	9.42E-04 (2.96%)	9.04E-04 (2.77%)	8.81E-04 (2.75%)
Liver	5.28E-02 (0.15%)	3.20E-02 (0.17%)	3.02E-02 (0.18%)	1.47E-01 (0.10%)	9.46E-02 (0.12%)	9.23E-02 (0.12%)	2.24E-01 (0.09%)	1.47E-01 (0.10%)	1.46E-01 (0.10%)
Esophagus	2.86E-01 (0.17%)	1.99E-01 (0.19%)	1.89E-01 (0.19%)	6.21E-01 (0.12%)	4.51E-01 (0.13%)	4.39E-01 (0.13%)	8.65E-01 (0.11%)	6.38E-01 (0.11%)	6.26E-01 (0.12%)
Thyroid	2.01E-02 (1.15%)	1.62E-02 (1.15%)	1.70E-02 (1.13%)	6.24E-02 (0.70%)	5.16E-02 (0.69%)	5.46E-02 (0.67%)	9.63E-02 (0.58%)	8.06E-02 (0.57%)	8.85E-02 (0.55%)
Gonads	1.95E-05 (33.68%)	1.80E-05 (32.57%)	1.70E-05 (41.80%)	8.06E-05 (17.94%)	6.34E-05 (17.13%)	6.93E-05 (16.07%)	1.87E-04 (11.03%)	1.68E-04 (10.87%)	1.45E-04 (11.45%)
Skin	1.08E-01 (0.02%)	9.45E-02 (0.02%)	8.59E-02 (0.02%)	1.29E-01 (0.02%)	1.13E-01 (0.02%)	1.01E-01 (0.02%)	1.42E-01 (0.02%)	1.24E-01 (0.02%)	1.11E-01 (0.02%)
Brain	3.03E-04 (2.24%)	2.68E-04 (2.08%)	2.54E-04 (2.14%)	1.19E-03 (1.26%)	1.23E-03 (1.10%)	1.21E-03 (1.11%)	2.27E-03 (0.96%)	2.35E-03 (0.84%)	2.36E-03 (0.83%)
Kidneys	1.59E-02 (0.49%)	1.35E-02 (0.47%)	1.32E-02 (0.48%)	4.81E-02 (0.31%)	4.22E-02 (0.29%)	4.25E-02 (0.29%)	7.43E-02 (0.25%)	6.62E-02 (0.24%)	6.78E-02 (0.24%)
Salivary glands	1.73E-03 (1.96%)	1.61E-03 (1.82%)	1.66E-03 (1.82%)	6.29E-03 (1.12%)	6.21E-03 (0.99%)	6.49E-03 (0.98%)	1.06E-02 (0.89%)	1.07E-02 (0.78%)	1.13E-02 (0.77%)
Adrenals	6.79E-02 (0.63%)	5.44E-02 (0.62%)	5.26E-02 (0.63%)	1.71E-01 (0.42%)	1.39E-01 (0.42%)	1.39E-01 (0.42%)	2.46E-01 (0.36%)	2.04E-01 (0.35%)	2.05E-01 (0.35%)
Gall bladder	1.40E-02 (1.01%)	9.95E-03 (1.06%)	9.38E-03 (1.09%)	4.87E-02 (0.59%)	3.73E-02 (0.60%)	3.65E-02 (0.61%)	8.07E-02 (0.47%)	6.25E-02 (0.48%)	6.20E-02 (0.48%)
Heart wall	6.57E-01 (0.06%)	5.00E-01 (0.06%)	4.70E-01 (0.06%)	1.26E+00 (0.05%)	9.99E-01 (0.05%)	9.55E-01 (0.05%)	1.66E+00 (0.04%)	1.35E+00 (0.04%)	1.30E+00 (0.04%)
Prostate	2.51E-05 (29.03%)	1.46E-05 (33.38%)	2.38E-05 (36.26%)	1.78E-04 (14.72%)	1.91E-04 (12.85%)	1.16E-04 (15.93%)	4.43E-04 (9.20%)	3.34E-04 (9.44%)	2.89E-04 (10.73%)
SI wall	1.75E-03 (0.70%)	1.47E-03 (0.67%)	1.45E-03 (0.68%)	7.48E-03 (0.39%)	6.50E-03 (0.37%)	6.72E-03 (0.36%)	1.32E-02 (0.30%)	1.17E-02 (0.29%)	1.23E-02 (0.28%)
Spleen	5.52E-01 (0.12%)	4.39E-01 (0.12%)	414E-01 (0.12%)	9.79E-01 (0.09%)	8.11E-01 (0.09%)	7.86E-01 (0.09%)	1.24E+00 (0.09%)	1.04E+00 (0.08%)	1.02E+00 (0.09%)
Thymus	9.22E-02 (0.44%)	6.88E-02 (0.46%)	6.74E-02 (0.46%)	2.28E-01 (0.30%)	1.77E-01 (0.31%)	1.79E-01 (0.31%)	3.27E-01 (0.26%)	2.59E-01 (0.26%)	2.66E-01 (0.26%)
Breasts	5.57E-02 (0.38%)	3.35E-02 (0.45%)	1.36E-02 (0.70%)	1.46E-01 (0.26%)	9.28E-02 (0.29%)	4.58E-02 (0.42%)	2.22E-01 (0.22%)	1.43E-01 (0.25%)	7.49E-02 (0.34%)
ET region	1.55E-02 (1.11%)	1.24E-02 (1.10%)	1.28E-02 (1.09%)	4.58E-02 (0.69%)	3.83E-02 (0.67%)	4.04E-02 (0.65%)	7.07E-02 (0.57%)	5.94E-02 (0.55%)	6.42E-02 (0.53%)
Oral mucosa	9.86E-04 (6.35%)	9.44E-04 (5.76%)	9.79E-04 (6.10%)	4.16E-03 (3.46%)	4.39E-03 (3.08%)	4.28E-03 (3.20%)	7.33E-03 (2.65%)	7.72E-03 (2.34%)	7.81E-03 (2.49%)
Pancreas	8.59E-03 (0.93%)	7.29E-03 (0.90%)	6.86E-03 (0.91%)	3.19E-02 (0.53%)	2.79E-02 (0.50%)	2.79E-02 (0.51%)	5.35E-02 (0.42%)	4.75E-02 (0.40%)	4.76E-02 (0.40%)
Bone marrow	8.44E-02 (0.69%)	5.49E-02 (0.65%)	5.34E-02 (0.81%)	1.75E-01 (0.38%)	1.15E-01 (0.34%)	1.14E-01 (0.38%)	2.50E-01 (0.28%)	1.65E-01 (0.26%)	1.65E-01 (0.27%)
Bone surfaces	6.60E-02 (1.82%)	4.21E-02 (1.62%)	4.13E-02 (2.15%)	1.34E-01 (1.26%)	8.83E-02 (1.13%)	8.80E-02 (1.36%)	1.82E-01 (0.97%)	1.22E-01 (0.85%)	1.22E-01 (1.02%)
Effective dose	1.53E-01 (2.75%)	1.20E-01 (2.66%)	1.11E-01 (3.40%)	2.89E-01 (1.46%)	2.31E-01 (1.39%)	2.18E-01 (1.31%)	3.85E-01 (0.90%)	3.09E-01 (0.89%)	2.94E-01 (0.93%)

Table 6. Net influence of body size on heart wall dose. Net influence is defined as the product of two factors. The first factor is the ratio of the dose to the detector-side DAP meter which highlights the influence of the ABC system. Each ratio represents the detector-side DAP dose normalized by the corresponding value for the 50th percentile phantom. The second factor is the ratio of the heart dose conversion coefficient. Again, each ratio represents the heart dose conversion coefficient normalized by the corresponding value for the 50th percentile phantom.

Projection	kVp	Ratio of dose at the detector-side DAP meter UFHADM mass percentile			Ratio of heart dose conversion coefficients UFHADM mass percentile			Net influence of body size on patient dose UFHADM mass percentile		
		10%	50%	90%	10%	50%	90%	10%	50%	90%
AP	60	0.51	1.00	2.24	1.17	1.00	0.47	0.60	–	1.05
	90	0.57	1.00	1.95	1.15	1.00	0.55	0.66	–	1.08
	120	0.60	1.00	1.87	1.14	1.00	0.59	0.68	–	1.10
PA	60	0.51	1.00	2.15	1.52	1.00	0.95	0.77	–	2.05
	90	0.58	1.00	1.90	1.42	1.00	0.97	0.82	–	1.84
	120	0.61	1.00	1.82	1.37	1.00	0.97	0.83	–	1.77
LAO	60	0.52	1.00	1.97	1.44	1.00	0.95	0.75	–	1.88
	90	0.57	1.00	1.73	1.38	1.00	0.97	0.79	–	1.68
	120	0.60	1.00	1.65	1.35	1.00	0.98	0.81	–	1.61
RAO	60	0.60	1.00	2.38	1.31	1.00	0.94	0.79	–	2.24
	90	0.65	1.00	2.01	1.26	1.00	0.96	0.82	–	1.93
	120	0.67	1.00	1.91	1.24	1.00	0.96	0.83	–	1.84

increase was most dramatic during AP projections where the phantoms differed most in the thickness of subcutaneous fat located superficial to major target organs. Second, the dose to the detector-side DAP meter also increased when total body mass decreased. This was due to a reduction in the overall amount of attenuating material. In this case, the increase was more uniform across beam angles. Third, organ and effective dose conversion coefficients increased when the tube potential was increased. Here, photons were able to penetrate further and deliver a higher dose to deep seated tissues. The relative change was largest for well-shielded organs such as the breast during PA projections. A final general trend was an increase in the dose to the detector-side DAP meter as tube potential increased. As expected, a higher energy spectrum meant that more x-rays were able to penetrate the patient and deliver dose to the DAP meter.

The net influence of body size on patient dose can be defined by the product of two factors. The first is the effect of the automatic brightness control (ABC) system. In real fluoroscopy systems, the ABC adjusts tube current and voltage to maintain a certain image quality as defined by indicators such as contrast and signal-to-noise ratio. These indicators are related to the energy and fluence of photons reaching the detector. As such, the dose to the detector-side DAP meter was used as an analogue for image quality in this research. The dose at the detector-side DAP meter for each 50th percentile phantom was then used as a benchmark for this analogue. The second factor is the change in the organ and effective dose conversion coefficients owing to differences in patient morphometry. The influences of both factors are shown in table 6 for the dose to the heart wall. Data are displayed for each Monte Carlo run as ratios normalized by their respective values for the patient at the 50th mass percentile. Taking as an example the Monte Carlo run for a 60 kVp AP projection,

Table 7. Relative error when patient size is neglected. All values were calculated as the per cent difference between the 10th and the 50th percentile DCCs and the 90th and 50th percentile DCCs, respectively.

	60 kVp		90 kVp		120 kVp	
	UFHADM mass percentile		UFHADM mass percentile		UFHADM mass percentile	
	10%	90%	10%	90%	10%	90%
AP						
Heart	-14.8%	112.9%	-13.0%	81.5%	-12.1%	70.2%
Liver	-24.0%	59.7%	-20.9%	39.5%	-19.5%	32.8%
Stomach	-20.6%	68.4%	-16.4%	46.9%	-14.7%	39.7%
Lung	-39.7%	95.5%	-35.2%	65.6%	-33.3%	55.5%
Esophagus	-31.1%	102.7%	-25.1%	76.8%	-23.1%	66.8%
Effective dose	-43.0%	43.2%	-37.4%	36.5%	-35.0%	33.1%
PA						
Heart	-34.1%	4.8%	-29.3%	3.5%	-27.2%	2.9%
Liver	-48.1%	2.7%	-39.5%	1.0%	-36.0%	0.1%
Stomach	-31.5%	5.8%	-26.2%	3.1%	-24.0%	2.3%
Lung	-34.1%	3.4%	-31.4%	1.8%	-30.0%	1.2%
Esophagus	-33.4%	3.9%	-25.7%	3.1%	-22.7%	2.7%
Effective dose	-34.5%	6.8%	-30.7%	5.4%	-29.0%	4.9%
LAO						
Heart	-30.8%	4.8%	-27.4%	3.2%	-25.8%	2.3%
Liver	-22.9%	8.3%	-19.3%	5.4%	-17.7%	4.3%
Stomach	-45.5%	4.5%	-39.3%	1.9%	-36.6%	0.5%
Lung	-19.8%	5.4%	-18.4%	3.8%	-17.7%	3.0%
Esophagus	-26.1%	4.7%	-21.9%	3.6%	-20.0%	2.9%
Effective dose	-23.2%	6.6%	-22.0%	5.0%	-21.4%	4.2%
RAO						
Heart	-23.8%	6.5%	-20.6%	4.5%	-19.1%	3.7%
Liver	-39.3%	6.0%	-35.6%	2.5%	-34.2%	1.1%
Stomach	-18.4%	8.6%	-14.8%	5.4%	-13.3%	4.2%
Lung	-17.3%	5.5%	-16.5%	3.6%	-16.1%	2.8%
Esophagus	-30.6%	5.0%	-27.4%	2.8%	-26.2%	1.9%
Effective dose	-21.5%	7.9%	-20.6%	6.0%	-19.8%	%

table 6 shows that compared to a 50th percentile individual, the heart dose conversion coefficient will be 17% higher for a 10th percentile patient, but the amount of radiation delivered to the patient will be roughly 50% lower. The product of the two ratios defines the net influence on patient dose and is shown in the final columns of table 6. As shown, for each Monte Carlo run the overweight patient receives a higher dose while the underweight patient receives a lower dose as compared to an average weight individual. Furthermore, it can be seen that if only a 50th percentile DCC is available, the DCC ratios will become uniform and the dose to the patient will be incorrectly estimated. The relative error associated with this simplification is highlighted in table 7 for several organs and was calculated as the per cent difference between the 10th and the 50th percentile DCCs and the 90th and 50th percentile DCCs, respectively. As seen in table 7, relative error can be as large as 113% for certain projections and in all cases the organ dose to an underweight patient will be underestimated and the organ dose to an overweight patient overestimated if patient size is neglected.

Table 8. Comparison of effective dose conversion coefficients for KTMAN-2 and the UFHADM patient-dependent series. Values in parenthesis represent effective dose with breast dose excluded.

		Effective dose conversion coefficient (mSv per Gy cm ²)			
		KTMAN-2	UFHADM ₅₀₋₁₀	UFHADM ₅₀₋₅₀	UFHADM ₅₀₋₉₀
Projection	kVp				
AP	60	0.17	0.37 (0.14)	0.21 (0.10)	0.15 (0.05)
	90	0.26	0.55 (0.26)	0.34 (0.20)	0.25 (0.12)
	120	0.36	0.67 (0.27)	0.43 (0.27)	0.33 (0.18)
PA	60	0.11	0.14	0.09	0.08
	90	0.22	0.28	0.19	0.18
	120	0.30	0.38	0.27	0.25
LAO	60	0.17	0.14	0.11	0.10
	90	0.33	0.27	0.21	0.20
	120	0.44	0.36	0.28	0.27
RAO	60	0.18	0.15	0.12	0.11
	90	0.35	0.29	0.23	0.22
	120	0.47	0.38	0.31	0.29

4. Discussion

As body size was shown to have a clear impact on patient dosimetry, an attempt was next made to compare calculated DCCs with those published by Park *et al* (2008) and to investigate whether DCCs could be selected for KTMAN-2 based only on his total body mass. A summary of this comparison is shown in table 8 which includes effective dose conversion coefficients selected from each study. While similar exam parameters were used for both studies, there were a number of differences in method which made such a comparison difficult. These included the use of different tissue weighting factors (ICRP 60 versus ICRP 103), a different scheme for calculating RBM and BS dose (numeric sum of individual homogeneous bone doses versus weighted average), and the absence of a breast target in the KTMAN-2 study. As mentioned previously, breast dose represented a major contributor to the effective dose for all AP projections. In order to make a better comparison, two values are listed in table 8 for these projections—one including breast dose and one excluding it.

In general, the DCCs published for KTMAN-2 aligned best with those calculated for the lower weight UFHADM₅₀₋₁₀ phantom. This follows from the fact that KTMAN-2 has a total body mass of only 68 kg which compares best with the 64.1 kg total body mass of the UFHADM₅₀₋₁₀. However, if total body mass was strictly used as a matching parameter, the DCCs for KTMAN-2 would fall somewhere between those of the underweight and average U.S. phantoms which was not the case for every projection. While this type of comparison provides some insight into the effectiveness of phantom-patient matching, it represents only a single test case, and one in which the *patient-specific* phantom (Korean-based KTMAN-2) did not share the same anthropometric origins of the *patient-dependent* phantoms (American-based UFHADM series). In order to further investigate the accuracy of phantom-patient matching based on anthropometric measurements, a larger study should be performed which would include a large number of patient-specific phantoms and a rich library of patient-dependent phantoms. As demonstrated in this work, hybrid phantoms are uniquely suited for this type of study.

While it was not the goal of this research to establish a definite link between any specific patient parameter and organ dose, it has been shown that organ and effective dose conversion coefficients are clearly influenced by patient size. More specifically, the level of disagreement between the DCCs of different sized phantoms appears to depend upon tube angle and whether a patient's weight gain (over reference anatomy) is localized between major organs and the x-ray tube, or major organs and the image detector. This can be seen most drastically when considering the differences between AP and PA projections. In both cases, the total body thickness remains the same, but the organ location relative to the entrance surface changes. For AP projections, the distance between the heart and the anterior surface was 6.5 cm for the underweight phantom, 7.9 cm for the average phantom and 11.3 cm for the overweight phantom. Consequently, the DCCs for each phantom were very different leading to large errors if patient size is neglected. For PA projections, the scenario is quite different. In this case, the distance between the heart and the posterior surface was 11.5 cm for the underweight phantom, 16.5 cm for the average phantom and only 16.7 cm for the overweight phantom. Due to the fact that there was little difference between the posterior weight gain of the average and overweight phantoms, the relative error in the effective dose was reduced by a factor of 7.

While great care was given to the parameterization of the terms underweight, average and overweight, tertiary parameters which were not considered, such as sub-scapular skin fold thickness, may have played a large role in more accurately defining the phantoms in key anatomic areas. For the case of cardiac catheterization, key areas would have included the upper torso, but for different studies these areas will change as will the anthropometric measurements which describe them. These findings indicate that organ and even effective dose conversion coefficients are sensitive to anthropometric changes and, more specifically, sensitive to local changes which affect the amount of subcutaneous fat situated between major organs and the x-ray tube.

5. Conclusions

Organ and effective dose conversion coefficients have been calculated using hybrid phantoms representing an underweight, average and overweight American adult male. Reference body sizes were determined using the NHANES III database and parameterized based on standing height and total body mass. Several general trends were observed when body size was decreased including an increase in the organ and effective dose conversion coefficients and an increase in the dose to the detector-side DAP meter. For a given image quality, it was shown that overweight patients receive higher doses and underweight patients lower doses when compared with the average individual. It was also shown that if patient size is neglected when choosing dose conversion coefficients, relative error as large as 113% can be encountered.

In order to briefly investigate the effectiveness of phantom-patient matching, the effective dose conversion coefficients calculated with the UFHADM series were compared with those published for the Korean voxel phantom KTMAN-2. While there were a number of dissimilarities in the way effective dose was calculated for each study, the DCCs published from KTMAN-2 aligned best with the UFHADM phantom which most closely matched in overall body size. Further investigation was recommended to determine general trends from a larger population and a more diverse library of patient-dependent hybrid phantoms.

By analyzing the DCCs of different projections, it was noted that DCCs show a strong dependence on beam angle resulting from changes in the amount of soft tissue located between organs and the x-ray tube. As patients gain weight, subcutaneous fat is added non-uniformly

along the tube/detector axis, and it was suggested that DCCs may be most closely dependent on anthropometric parameters that best describe weight gain in key areas along this axis. Hybrid phantoms offer unique advantages to investigate these types of scenarios and will be used in the future to expand upon the findings of this research study.

Acknowledgments

This work was performed under grant RO1 CA116743 from the National Cancer Institute (subcontract by the Rensselaer Polytechnic Institute) with the University of Florida. This work was supported by the National Cancer Institute

References

- Bozkurt A and Bor D 2007 Simultaneous determination of equivalent dose to organs and tissues of the patient and of the physician in interventional radiology using the Monte Carlo method *Phys. Med. Biol.* **52** 317–30
- Cranley K, Gilmore B J, Fogarty G W A and Desponds L 1997 Catalogue of diagnostic x-ray spectra and other data *Report No. 78* (London: The Institute of Physics)
- Eckerman K F 1985 Aspects of the dosimetry of radionuclides within the skeleton with particular emphasis on the active marrow *Proc. 4th Int. Radiopharmaceutical Dosimetry Symp.* ed A T Schlafke-Stelson and E E Watson (Oak Ridge, TN: Oak Ridge Associated Universities) pp 514–34
- Eckerman K F, Bolch W E, Zankl M and Petoussi-Henss N 2008 Response functions for computing absorbed dose to skeletal tissues for photon irradiation *Radiat. Prot. Dosim.* **127** 187–91
- Hart D, Jones D G and Wall B F 1994 Estimation of effective dose in diagnostic radiology from entrance surface dose and dose-area product measurement *NRPB-R262* (Chilton: National Radiological Protection Board)
- ICRP 2002 ICRP Publication 89: basic anatomical and physiological data for use in radiological protection—reference values *Ann. ICRP* **32** 1–277
- ICRP 2007 ICRP Publication 103: recommendations of the International Commission on Radiological Protection *Ann. ICRP* **37** 1–332
- ICRU 1992 Photon, electron, proton and neutron interaction data for body tissues *Report 46* (Bethesda, MD: International Commission on Radiation Units and Measurements)
- Lee C, Lee C and Bolch W 2006a Age-dependent organ and effective dose coefficients for external photons: a comparison of stylized and voxel-based pediatric phantoms *Phys. Med. Biol.* **51** 4663–88
- Lee C, Lee C, Park S H and Lee J K 2006b Development of the two Korean adult tomographic computational phantoms for organ dosimetry *Med. Phys.* **33** 380–90
- Lee C, Lodwick D, Hasenauer D, Williams J L, Lee C and Bolch W E 2007 Hybrid computational phantoms of the male and female newborn patient: NURBS-based whole-body models *Phys. Med. Biol.* **52** 3309–33
- Lee C, Lodwick D, Hurtado J L, Pafundi D H and Bolch W E 2008 Development of a series of hybrid computational phantoms and their applications to assessment of photon and electron specific absorbed fractions (abstract) *Eur. J. Nucl. Med.* **35** S202
- Park S H, Lee J K and Lee C 2008 Dose conversion coefficients calculated using tomographic phantom, KTMAN-2, for x-ray examination of cardiac catheterisation *Radiat. Prot. Dosim.* **128** 351–8
- Pelowitz D B 2005 MCNPX User's Manual Version 2.5.0 *Report LA-CP-05-0369* (Los Alamos, NM: Los Alamos National Laboratory)
- Schlattl H, Zankl M, Hausleiter J and Hoeschen C 2007 Local organ dose conversion coefficients for angiographic examinations of coronary arteries *Phys. Med. Biol.* **52** 4393–408
- Servomaa A, Rannikko S, Nikitin V, Golikov V, Ermakov I, Marsarskiy L and Saltukova L 1989 A topographically and anatomically unified phantom model for organ dose determination in radiation hygiene *Report STUK-A87* (Helsinki: Finnish Centre for Radiation and Nuclear Safety)
- Stern S H, Rosenstein M, Renaud L and Zankl M 1995 Handbook of selected tissue doses for fluoroscopic and cineangiographic examination of the coronary arteries *FDA Report 95-8288* (Rockville, MD: Food and Drug Administration)
- Tung C J, Lee C J, Tsai H Y, Tsai S F and Chen I J 2008 Body size-dependent patient effective dose for diagnostic radiography *Radiat. Meas.* **43** 1008–11
- Veit R and Zankl M 1992 Influence of patient size on organ doses in diagnostic radiology *Radiat. Prot. Dosim.* **43** 241–3

- Veit R and Zankl M 1993 Variation of organ doses in pediatric radiology due to patient diameter calculated with phantoms of varying voxel size *Radiat. Prot. Dosim.* **49** 353–6
- Veit R, Zankl M and Petoussi N 1989 Tomographic anthropomorphic models: I. Construction techniques and description of models of an 8-week-old baby and a 7-year-old child *GSF-Bericht 3/89* (Neuherberg: Gesellschaft für Strahlenforschung)
- Whalen S, Lee C, Williams J L and Bolch W E 2008 Anthropometric approaches and their uncertainties to assigning computational phantoms to individual patients in pediatric dosimetry studies *Phys. Med. Biol.* **53** 453–71